Nonlinear chiral magnetic waves

Kazuki Ikeda[1,2,*] Dmitri E. Kharzeev,[2,3,†] and Shuzhe Shi[4,2,‡]

[1]*Co-design Center for Quantum Advantage, Stony Brook University, Stony Brook, New York 11794-3800, USA*
[2]*Center for Nuclear Theory, Department of Physics and Astronomy, Stony Brook University, Stony Brook, New York 11794-3800, USA*
[3]*Department of Physics, Brookhaven National Laboratory, Upton, New York 11973-5000, USA*
[4]*Department of Physics, Tsinghua University, Beijing 100084, China*

The chiral magnetic wave (CMW) is a macroscopic quantum phenomenon that arises due to the mixing of the electric and chiral charge oscillations induced by the chiral anomaly. In this study we report the first quantum simulation (on classical hardware) of the real-time dynamics of CMWs in the Schwinger model. Our quench protocol is the following; at $t = 0$ we suddenly place an electric dipole at the middle of our lattice. Due to chiral anomaly, this dipole excites the CMW that propagates towards the edges of the lattice. In the Schwinger model tuned to the conformal critical point (at $\theta = \pi$, $m/g \simeq 0.2$), we find a gapless linear CMW that propagates with the speed of light. For a massless Schwinger model ($\theta = 0$, $m = 0$), we find a gapped linear CMW, in accord with previous analytical analyses. For a massive Schwinger model (that is dual to strongly interacting bosonic theory), we enter the new regime of nonlinear CMWs, where we find a surprise. Specifically, for $m/g > 1$, the frequency of electric charge oscillations becomes much smaller than the frequency of the oscillations of the chiral charge. For $m/g = 4$, we find a solution corresponding to a nearly static electric dipole with fast oscillations of the chiral charge confined within. We call this solution a "thumper" and study its properties in detail. We speculate that thumpers might be relevant for CMWs in the strange quark sector of quark-gluon plasma and narrow gap semiconductors.

I. INTRODUCTION

In the presence of an external magnetic field, the chirality imbalance (i.e., the difference in the densities of right- and left-handed fermions) induces an electric current directed along the direction of magnetic field—this is the chiral magnetic effect (CME) [1–3]; for reviews, see [4–7]. CME is an inherently nonequilibrium phenomenon stemming from the nonconservation of chiral charge dictated by the chiral anomaly. The nonequilibrium nature of CME becomes particularly apparent in the emergence of a collective chiral excitation stemming from the anomaly-induced coupling of chiral charge oscillations to the oscillations of electric charge; the chiral magnetic wave (CMW) [8].

It is instructive to investigate the physics of CMW in $(1 + 1)$ dimensional models, corresponding to the strong magnetic field limit of $(3 + 1)$ theories. In particular, the case of $(1 + 1)$-dimensional massless QED (Schwinger model) has been discussed already in [8]. As is well-known, massless Schwinger model is exactly solvable by bosonization, and its free-massive bosonic excitation can be interpreted as a result of mixing between the gauge field and the CMW [8].

In this paper, we will extend the analysis of the CMW to the massive Schwinger model. This model is interesting because it possesses confinement, and in bosonic representation describes nonlinear strongly interacting theory. Since the massive Schwinger model is not solvable analytically, and we are interested in the real-time, nonequilibrium behavior, we will rely on quantum simulations (on classical hardware). Many interesting aspects of $(1 + 1)$-dimensional quantum field theories have been successfully addressed using quantum simulations (see [9–17] for examples and [18] for a recent review of quantum simulation approach).

[*]kazuki.ikeda@stonybrook.edu
[†]dmitri.kharzeev@stonybrook.edu
[‡]shuzhe-shi@tsinghua.edu.cn

II. SCHWINGER MODEL

The Lagrangian density of the Schwinger model [19] is

$$\mathcal{L} = -\frac{1}{4}F_{\mu\nu}F^{\mu\nu} + \bar{\psi}(i\gamma^\mu\partial_\mu - g\gamma^\mu A_\mu - m)\psi. \quad (1)$$

We label the space-time coordinate by $x^\mu = (t, z)$. We denote the Pauli matrices as X, Y, and Z, and use the following convention for the Dirac matrices: $\gamma^0 = Z$, $\gamma^1 = iY$, $\gamma^5 = \gamma^0\gamma^1 = X$. In $(1+1)$ dimensions, the axial charge density $q_5(x) \equiv \bar\psi\gamma^5\gamma^0\psi(x)$ and the vector current density $j(x) \equiv \bar\psi\gamma^1\psi(x)$ are related by $q_5(x) = -j(x)$. Likewise, the vector charge density $q(x) \equiv \bar\psi\gamma^0\psi(x)$ and the axial current density $j_5(x) \equiv \bar\psi\gamma^5\gamma^1\psi(x)$ are related by $q(x) = j_5(x)$.

Because of these relations, the conservation of vector charge can be expressed as

$$\partial_t q - \partial_z q_5 = 0. \tag{2}$$

To obtain the equation for the CMW, we combine this relation with the conservation of axial charge $\partial_\mu J_5^\mu = 2im\bar\psi\gamma^5\psi$ (in the absence of an external electric field), and use the bosonization dictionary, in which $q \to -\frac{\partial_z\phi}{\sqrt\pi}$, $q_5 \to -\frac{\partial_t\phi}{\sqrt\pi}$, and $i\bar\psi\gamma^5\psi \to -cM\sin(2\sqrt\pi\phi)$, with $M = g/\sqrt\pi$ and $c = e^\gamma/(2\pi)$. The resulting equation describing the CMW in the Schwinger model then reads

$$(\partial_t^2 - \partial_z^2 + M^2)\phi + 2\sqrt\pi cmM\sin(2\sqrt\pi\phi) = 0. \tag{3}$$

It is clear that for the massless case $m = 0$, the equation is linear and describes the propagation of a gapped excitation with mass $M = g/\sqrt\pi$-this is a familiar noninteracting bosonic representation of the Schwinger model. The dispersion relation of this bosonic excitation can be derived as a result of mixing between the gapless CMW and a plasmon mode (see [8]). For massive case $m \neq 0$, the CMW equation becomes nonlinear. The case of $\theta = \pi$ can be obtained by flipping the sign of fermion mass, $m \to -m$. Near the critical point at $\theta = \pi$ and $m/g \simeq 0.3$ (in the continuum case), the potential in (3) becomes nearly flat, and the dynamics become close to conformal (see [17]). In this case, we expect to see a gapless linear CMW.

III. THE LATTICE HAMILTONIAN

To discretize our Hamiltonian, we use staggered fermions [20,21]

$$\psi_1(x) \to \frac{\chi_{2n}}{\sqrt a}, \qquad \psi_2(x) \to \frac{\chi_{2n+1}}{\sqrt a}, \tag{4}$$

where a is the finite lattice spacing. Then the lattice Hamiltonian corresponding to Eq. (1) is

$$H = -\frac{i}{2a}\sum_{n=1}^{N-1}[\chi_{n+1}^\dagger\chi_n - \chi_n^\dagger\chi_{n+1}]$$
$$+ m\sum_{n=1}^{N}(-1)^n\chi_n^\dagger\chi_n + \frac{ag^2}{2}\sum_{n=1}^{N-1}L_n^2, \tag{5}$$

where L_n is the electric field operator satisfying the Gauss' law constraint

$$L_n - L_{n-1} = \chi_n^\dagger\chi_n - \frac{1 - (-1)^n}{2}. \tag{6}$$

For the purpose of quantum simulation, let us put the lattice Hamiltonian in the spin representation using the Jordan-Wigner transformation [22],

$$\chi_n = \frac{X_n - iY_n}{2}\prod_{i=1}^{n-1}(-iZ_i). \tag{7}$$

The Hamiltonian of the model then becomes

$$H = \frac{1}{4a}\sum_{n=1}^{N-1}[X_nX_{n+1} + Y_nY_{n+1}]$$
$$+ \frac{m}{2}\sum_{n=1}^{N}(-1)^nZ_n + \frac{ag^2}{2}\sum_{n=1}^{N-1}L_n^2, \tag{8}$$

and the local vector and axial charge densities are, respectively,

$$Q_n \equiv \bar\psi\gamma^0\psi = \frac{Z_n + (-1)^n}{2a}, \tag{9}$$

$$Q_{5,n} \equiv \bar\psi\gamma^5\gamma^0\psi = \frac{X_nY_{n+1} - Y_nX_{n+1}}{4a}. \tag{10}$$

For later convenience, we define the total charge operator $Q \equiv a\sum_{n=1}^{N}Q_n$, which commutes with the Hamiltonian. With the boundary condition $L_0 = 0$, the Gauss' law constraint (6) leads to the solution

$$L_n = a\sum_{j=1}^{n}Q_j. \tag{11}$$

IV. THE QUENCH PROTOCOL

To study the real-time dynamics of CMW, we first prepare the ground state of the system and then perform a quench by introducing at time $t = 0$ an electric dipole at the center of our lattice. The time evolution is then described by the Hamiltonian (8).

To be more specific, the Hamiltonian (8) is a high-dimensional, yet sparse, matrix. We first obtain the vacuum state $|0\rangle$ as the Hamiltonian's ground state by exact diagonalization. Then at $t = 0$ we introduce the electric dipole at the center of our lattice. We truncate the Hilbert space by keeping a hundred of the lowest energy levels, and write the state at $t = 0$ as

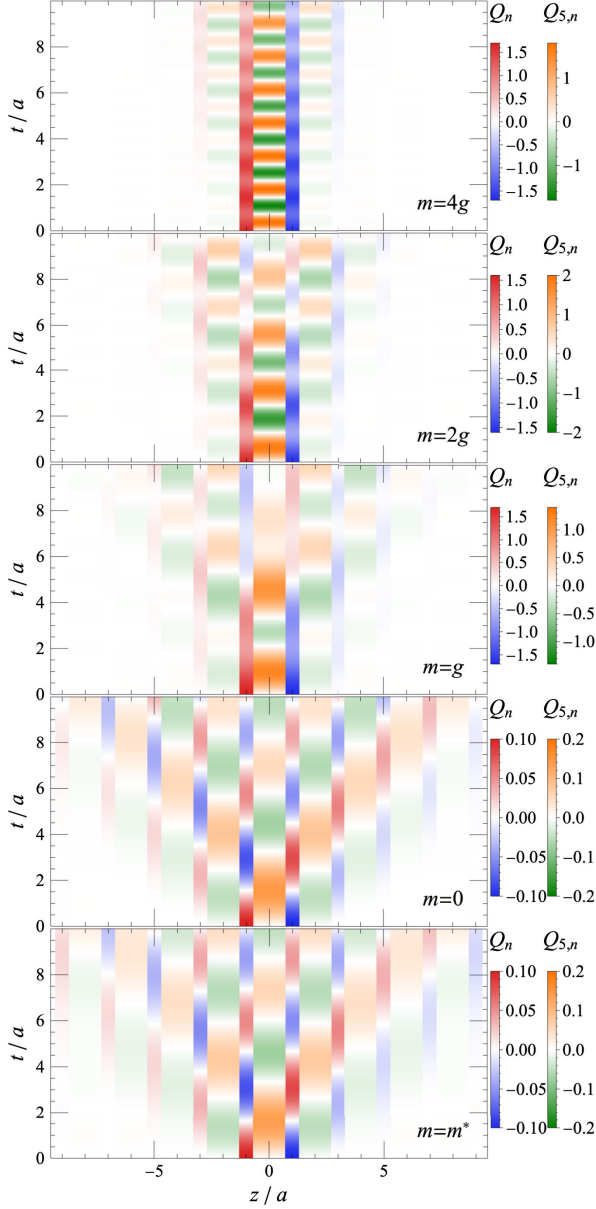$$|\psi\rangle_{t=0} = \sum_{k=0}^{N_{\text{trunc}}}c_k|k\rangle, \tag{12}$$

FIG. 1. (From top to bottom) Propagation of local electric charge and electric current for $m = 4g$, $m = 2g$, $m = g$, $m = 0$, and $m = m^* = -0.2g$. Expectation values of the vacuum states have been subtracted.

where the superposition coefficients are fixed so that the initial state contains a vector charge dipole on top of the vacuum,

$$\langle \psi | Q_n | \psi \rangle_{t=0} = \langle 0 | Q_n | 0 \rangle + D(\delta_{n,\frac{N}{2}} - \delta_{n,\frac{N}{2}+1}),$$

$$\langle \psi | Q_{5,n} | \psi \rangle_{t=0} = \langle 0 | Q_{5,n} | 0 \rangle. \quad (13)$$

Here, D is the magnitude of electric charges in the dipole, and we choose the coefficients so that D is maximized, within our truncated Hilbert space and on our lattice. With the initial state prepared, we evolve the quantum state

according to $|\psi\rangle_t = e^{-iHt}|\psi\rangle_{t=0}$, and measure the local and global observables as a function of time.

We set up the calculation with 20 staggered sites ($N = 20$), and take the lattice spacing as $a = 0.5/g$. We explore several values of the fermion mass; massive ($m = 4g$, $2g$, and g), massless ($m = 0$), and critical mass of the phase transition ($m = m^* = -0.2g$). For each of these values, we solve the vacuum state and time evolution and measure the local charges. Results are presented in Fig. 1. Here, we have combined the staggered fermion-antifermion pairs to obtain the physical vector charge density, i.e., $Q(z_n) = Q_{2n-1} + Q_{2n}$, whereas the axial charge is defined on the link between two sites, $Q_5(z_{n+1/2}) = 2Q_{5,2n}$. The charge conservation requirement (2), as manifested in staggered observables, $\partial_t Q_{2n-1} = (Q_{5,2n-1} - Q_{5,2n-2})/a$ and similarly for $\partial_t Q_{2n}$, automatically lead to the continuity equation,[1]

$$\partial_t Q(z_n) = \frac{Q_5(z_{n+1/2}) - Q_5(z_{n-1/2})}{2a}.$$

At each site, we observe oscillations of the local vector and axial charges, and these oscillations propagate from the middle of the lattice toward its edges forming a light cone structure. For the massive $m \neq 0$ scenario, we observe a stronger damping of the oscillation amplitude, compared to the massless and critical point scenarios. This can be attributed to the nonlinear nature of CMW in the massive case.

V. THUMPER SOLUTION

In particular, in the massive cases of $m = g$, $2g$, and $4g$, we observe that the oscillation period for vector charge is much longer than that of the axial charge, and the ratio between them increases with fermion mass. This is especially striking in the case of $m = 4g$ (see the upper panel of Fig. 1); the electric dipole is nearly static and does not oscillate at all, whereas the axial charge rapidly oscillates within the dipole. We refer to this solution as a "thumper". Unfortunately, so far we have not been able to find the corresponding classical solution of (3) analytically.

To understand the real-time evolution of the vector and axial charges in terms of the eigenstates of Hamiltonian,

$$H|k\rangle = E_k|k\rangle. \quad (14)$$

we start with the initial state

$$|\Psi(t = 0)\rangle = \sum_k c_k |k\rangle, \quad (15)$$

and consider the time dependence of an operator O in the Heisenberg picture

---

[1]Note that a physical site contains two lattice sites, therefore it has volume $2a$.
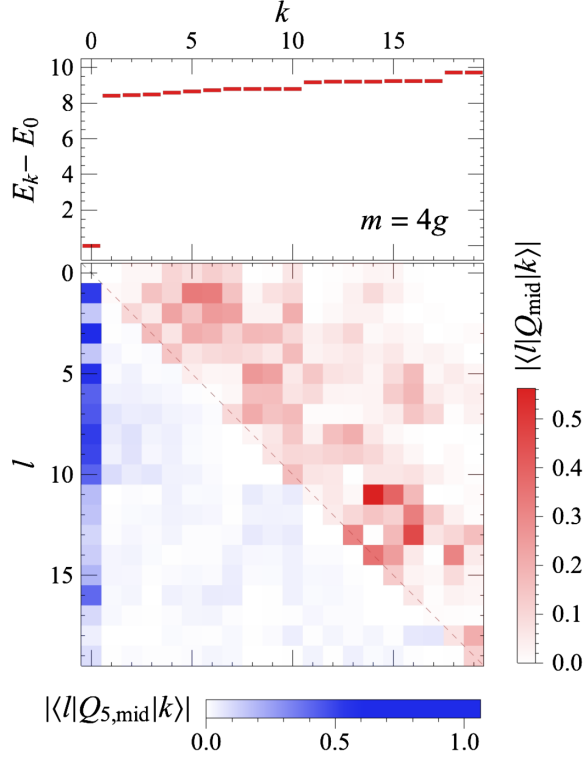
FIG. 2.   Energy level (upper) and modular of matrix elements (lower) for vector (upper triangle) and axial (lower triangle) charges. Note that $|\langle l|Q|k\rangle| = |\langle k|Q|l\rangle|$ and likewise for Q_5. Also, $|\langle k|Q_5|k\rangle| = 0$.

$$O(t) \equiv \langle \Psi(t)|O|\Psi(t)\rangle$$
$$= \sum_{k,l} c_l^* c_k e^{i(E_l - E_k)t}\langle l|O|k\rangle. \qquad (16)$$

It is a superposition of different oscillation modes. In each mode, the oscillation frequency is the difference between two energy eigenvalues. In Fig. 2, we show the energy eigenvalues and matrix elements for operators $Q_{\mathrm{mid}} \equiv Q(z_{N/2})$ and $Q_{5,\mathrm{mid}} \equiv Q_5(z_{(N+1)/2})$. While we have extracted 100 lowest energy states in the $Q = 0$ subspace, only those with nonvanishing overlap ($|c_k|^2$) with the initial states are presented in this plot. We note that all excited states are above the ground-state energy by $E_k - E_0 \gtrsim 2m$, which correspond to bound states consisting of a fermion-antifermion pair. Meanwhile, the energy difference between different excited states is of the order of $\mathcal{O}(g)$. From Fig. 2 (lower), it is clear that the axial charge operator is dominated by the excitation between the vacuum and the excited bound states (see leftmost column), whereas the vector charge operator is dominated by scattering between excitations. Therefore, in the massive limit that $2m \gg g$, the oscillation frequency of the axial charge is much greater than that of the vector charge. In the massless limit ($m = 0$) or critical mass $m = m^*$, there is no longer $\sim 2m$ mass gap between the vacuum and the bound states, and the axial and vector charges oscillate with the same frequency.

VI. CONCLUSION

We have presented the study of real-time dynamics of chiral magnetic waves (CMWs) in massless and massive Schwinger model using quantum simulations on a classical hardware. For Schwinger model tuned to the conformal critical point ($\theta = \pi$, $m/g \simeq 0.2$) we have observed a gapless CMW propagating with the speed of light. For massless case, we found a gapped CMW corresponding to the familiar noninteracting massive boson representation.

In the case of a massive Schwinger model ($m/g > 1$), we have uncovered the existence of novel "thumper" solutions in which the electric charge density oscillates much slower than the axial charge density. In particular, at $m/g = 4$ we have observed a nearly static electric dipole with rapid oscillations of chiral charge confined within. Qualitatively, this happens because at large m/g it becomes difficult to break the confining electric string between the charges in the dipole, which prevents the dipole from expanding. On the other hand, the interplay of chiral anomaly and the large fermion mass results in rapid oscillations of chiral charge inside the string. The confining electric string thus contains rapid fluctuations of chiral charge. It will be interesting to explore the possible link [23,24] between the fluctuations of topology and confinement in $(3 + 1)$ dimensions. It will also be interesting to explore the nonlinear CMWs and the "thumpers" in real systems.

Our results may be relevant for chiral magnetic waves in quark-gluon plasma and in condensed matter systems. Indeed, at strong magnetic field B the behavior of chiral magnetic waves was shown [25] to become effectively $(1 + 1)$ dimensional, with the dimensionful coupling $g^2 \equiv e \times eB/2\pi$. Assuming a magnetic field $eB \sim 10M_\pi^2$ (where M_π is the pion mass) at early moments of a heavy-ion collision justifies the reduction to $(1 + 1)$ dimensions since $\sqrt{eB} \simeq 3M_\pi > T$, where T is the temperature of the plasma. The corresponding dimensionful coupling is $g \simeq 0.25$ GeV. Therefore the dynamics of the chiral magnetic wave in the u, d quark sector is linear, but it does become nonlinear in the strange quark sector, with the mass of the s quark $m_s \sim g$. Therefore, when the experimental studies of chiral magnetic waves are extended to strange hadrons, they have to take into account the nonlinear dynamics of the chiral magnetic wave studied here.

In the case of condensed matter physics, nonlinear dynamics of chiral magnetic waves can be studied in narrow gap semiconductors, with gap Δ, for magnetic fields satisfying $(2\pi/e)\Delta^2 > eB > T^2$, where T is the temperature. The first of these inequalities enforces the nonlinear regime, and the second enforces the validity of dimensional reduction.

ACKNOWLEDGMENTS

APPENDIX: EIGENSTATE ANALYSIS OF OSCILLATIONS IN VECTOR AND AXIAL CHARGES

For completeness, we present the energy eigenvalues and the matrix elements of vector and axial charge operators for fermion mass $m = 2g$, g, 0, and critical mass m^*.
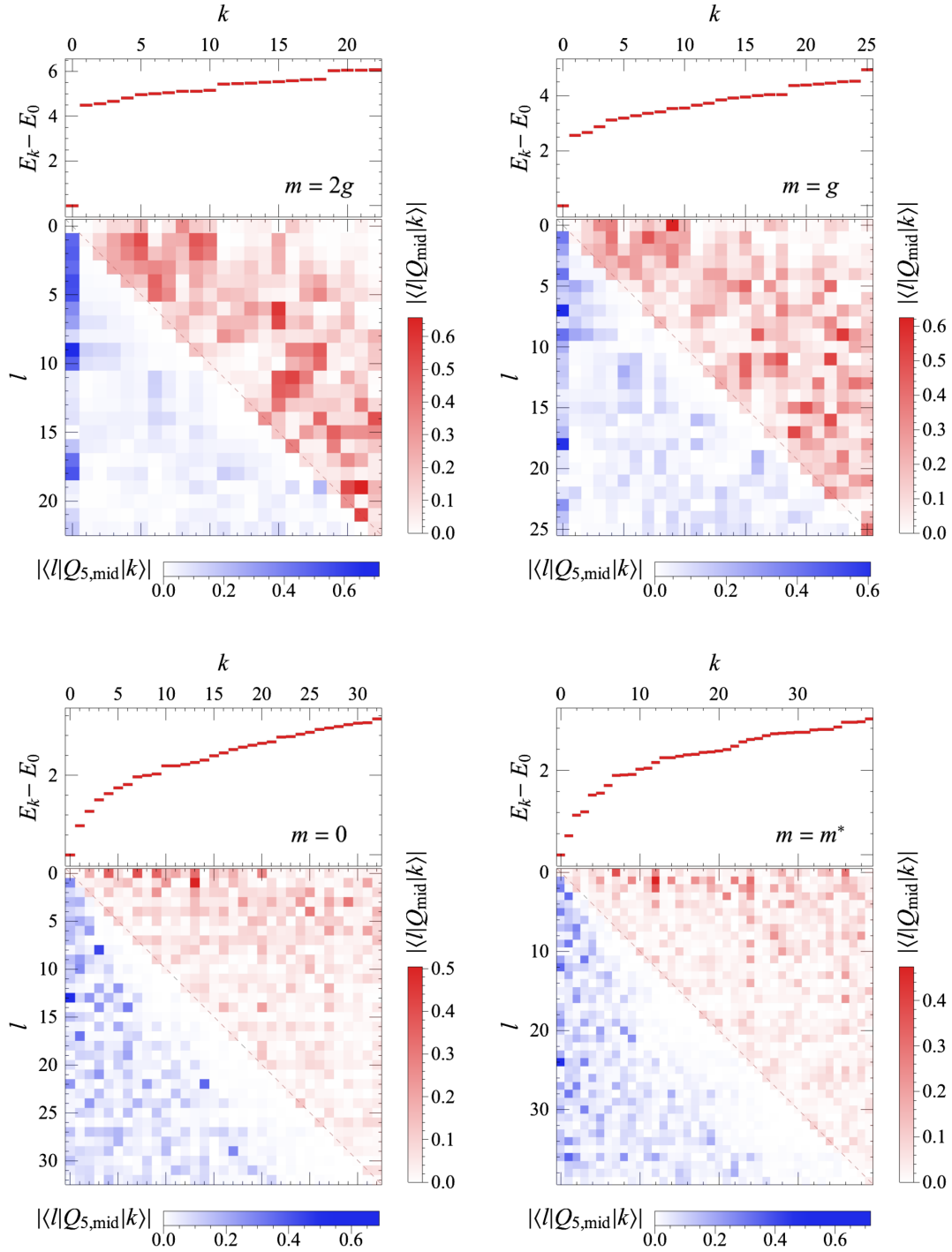

FIG. 3.   Same as Fig. 2 of the main text but for masses $m = 2g$ (upper left), g (upper right), 0 (lower left), and m^* (lower right).

[1] D. Kharzeev, Parity violation in hot QCD: Why it can happen, and how to look for it, Phys. Lett. B **633,** 260 (2006).

[2] D. E. Kharzeev, L. D. McLerran, and H. J. Warringa, The effects of topological charge change in heavy ion collisions: event by event p and cp violation, Nucl. Phys. **A803,** 227 (2008).

[3] K. Fukushima, D. E. Kharzeev, and H. J. Warringa, The chiral magnetic effect, Phys. Rev. D **78,** 074033 (2008).

[4] D. E. Kharzeev, The chiral magnetic effect and anomaly-induced transport, Prog. Part. Nucl. Phys. **75,** 133 (2014).

[5] D. E. Kharzeev, J. Liao, S. A. Voloshin, and G. Wang, Chiral magnetic and vortical effects in high-energy nuclear collisions—A status report, Prog. Part. Nucl. Phys. **88,** 1 (2016).

[6] K. Landsteiner, Notes on anomaly induced transport, Acta Phys. Pol. B **47,** 2617 (2016).

[7] D. E. Kharzeev and J. Liao, Chiral magnetic effect reveals the topology of gauge fields in heavy-ion collisions, Nat. Rev. Phys. **3,** 55 (2021).

[8] D. E. Kharzeev and H.-U. Yee, Chiral magnetic wave, Phys. Rev. D **83,** 085007 (2011).

[9] N. Klco, E. F. Dumitrescu, A. J. McCaskey, T. D. Morris, R. C. Pooser, M. Sanz, E. Solano, P. Lougovski, and M. J. Savage, Quantum-classical computation of Schwinger model dynamics using quantum computers, Phys. Rev. A **98,** 032331 (2018).

[10] N. Butt, S. Catterall, Y. Meurice, R. Sakai, and J. Unmuth-Yockey, Tensor network formulation of the massless Schwinger model with staggered fermions, Phys. Rev. D **101,** 094509 (2020).

[11] G. Magnifico, M. Dalmonte, P. Facchi, S. Pascazio, F. V. Pepe, and E. Ercolessi, Real time dynamics and confinement in the $\mathbb{Z}_n$ Schwinger-Weyl lattice model for $1 + 1$ QED, Quantum **4,** 281 (2020).

[12] A. F. Shaw, P. Lougovski, J. R. Stryker, and N. Wiebe, Quantum algorithms for simulating the lattice Schwinger model, Quantum **4,** 306 (2020).

[13] D. E. Kharzeev and Y. Kikuchi, Real-time chiral dynamics from a digital quantum simulation, Phys. Rev. Res. **2,** 023342 (2020).

[14] K. Ikeda, D. E. Kharzeev, and Y. Kikuchi, Real-time dynamics of Chern-Simons fluctuations near a critical point, Phys. Rev. D **103,** L071502 (2021).

[15] A. Florio, D. Frenklakh, K. Ikeda, D. Kharzeev, V. Korepin, S. Shi, and K. Yu, Real-Time Nonperturbative Dynamics of Jet Production in Schwinger Model: Quantum Entanglement and Vacuum Modification, Phys. Rev. Lett. **131,** 021902 (2023).

[16] K. Ikeda, Criticality of quantum energy teleportation at phase transition points in quantum field theory, Phys. Rev. D **107,** L071502 (2023).

[17] K. Ikeda, D. E. Kharzeev, R. Meyer, and S. Shi, Detecting the critical point through entanglement in Schwinger model, arXiv:2305.00996.

[18] C. W. Bauer *et al.*, Quantum simulation for high energy physics, PRX Quantum **4,** 027001 (2023).

[19] J. S. Schwinger, Gauge invariance and mass. 2., Phys. Rev. **128,** 2425 (1962).

[20] J. B. Kogut and L. Susskind, Hamiltonian formulation of Wilson's lattice gauge theories, Phys. Rev. D **11,** 395 (1975).

[21] L. Susskind, Lattice fermions, Phys. Rev. D **16,** 3031 (1977).

[22] P. Jordan and E. P. Wigner, About the Pauli exclusion principle, Z. Phys. **47,** 631 (1928).

[23] D. E. Kharzeev and E. M. Levin, Color Confinement and Screening in the θ Vacuum of QCD, Phys. Rev. Lett. **114,** 242001 (2015).

[24] D. E. Kharzeev, Color confinement from fluctuating topology, Int. J. Mod. Phys. A **31,** 1645023 (2016).

[25] D. E. Kharzeev and H.-U. Yee, Chiral magnetic wave, Phys. Rev. D **83,** 085007 (2011).